Secondary Ion Mass Spectrometry of Molecular Solids. Cluster Formation during Ion Bombardment of Frozen Water, Benzene, and Cyclohexane

Gerald M. Lancaster,† Fumihiro Honda, Yasuo Fukuda, and J. W. Rabalais*

Contribution from the Department of Chemistry, University of Houston, Houston, Texas 77004. *Received August 30, 1978*

Abstract: The secondary ion mass spectra (SIMS) of H_2O, C_6H_6, and C_6H_{12} frozen at 77 K are reported. The spectra are generated by subjecting the molecular surface to 0.5–3-keV He^+ ions and mass analyzing the positive and negative secondary clusters in a quadrupole mass filter. The most abundant clusters in the H_2O spectrum were of the type $H(H_2O)_n^+$, $n = 1, 2, \ldots, 51$, although other low-intensity clusters were also observed. The benzene and cyclohexane spectra exhibited clusters of the type $C_nH_m^+$, $n = 1, 2, \ldots, 32$ and $m = 1, 2, \ldots, 10$. The intensities I of the different types of cluster series observed from H_2O vary as a function of the number of H_2O molecules n in the cluster according to $I = ae^{bn}$ where a and b are constants. The kinetic energy distributions of the clusters have a maximum in the region 1.0–3.3 eV which, in general, shifts to lower energy and sharpens with increasing cluster size. A general clustering mechanism which is qualitatively consistent with all of the experimental observations is proposed. This mechanism involves thermal activation by the primary ion impact and irreversible adiabatic expansion to relieve the nonequilibrium situation. Bound clusters are formed from collections of secondary particles moving through the selvedge region of the surface. The formation of a tightly bound cluster only as the particles are moving through the surface accounts for the molecular rearrangement observed during sputtering.

I. Introduction

In secondary ion mass spectrometry (SIMS) a solid sample is bombarded by primary ions with typically a few kiloelectron volts kinetic energy. The energy transferred to the surface results in the sputtering of secondary atoms, molecules, and clusters in the form of positive, negative, and neutral species with energies in the electron volt region. Using electrostatic lenses, the ions can be drawn into a mass spectrometer for mass analysis under ultrahigh-vacuum conditions yielding an extremely sensitive elemental analysis of the surface. The successful application of SIMS to chemical structure analysis is restricted by the lack of information on two basic processes, i.e., the degree to which the detected secondary ion clusters reflect the virgin surface structure and the mechanism of cluster formation in sputtering. Investigations of molecular solids using SIMS have only recently begun,[1-6] whereas applications to metals,[7,8] chemisorption studies,[9-12] and depth concentration profiling[13] are more advanced. The theory of surface sputtering by ion beams has been studied extensively;[14] however, the mechanism of cluster formation remains obscure.[15] The dynamics of an ion bombarded solid[16] and the mechanism of formation of small metal clusters[17,18] have been examined using computer-simulated classical trajectory methods.

This paper presents a SIMS study of three molecular solids, i.e., H_2O, C_6H_6, and C_6H_{12}, maintained at 77 K. As part of our program for investigating the mechanism of formation and production of large molecular clusters in the sputtering process, the objectives of this paper are as follows. We seek to exploit the suitability of SIMS for characterization of molecular solids, to measure kinetic energy distributions of the emitted secondary ions, to determine the influence of primary ion energy on the abundance of secondary ions, and to develop a general mechanism for cluster formation. This is the first SIMS study of frozen H_2O and cyclohexane and the first SIMS measurement on benzene to be carried out to high masses. The first SIMS study[1] of frozen benzene was carried out only to m/e ~80. The observation of ion clusters with mass up to 919 amu containing 154 atoms, e.g., $H(H_2O)_{51}^+$, represents the largest cluster ions that have been produced by sputtering and detected by SIMS to date. Large water clusters of the type $H(H_2O)_n^+$ have been produced previously[19] by adiabatic expansion of water vapor in supersonic jets and the kinetics and thermodynamic properties of clusters with $n = 1, 2, \ldots, 8$ have been studied.[20] A recent SIMS study[21] of the adsorption of H_2O on alkali halide surfaces revealed clusters of the type $H(H_2O)_n^+$, $n = 1, 2, \ldots, 13$, as well as other types. Electron-stimulated,[22] molecular beam,[23] and mass spectrometric[24] measurements have revealed small water clusters of various types.

II. Experimental Methods

The details of the design of the SIMS system and pumping facilities have been described elsewhere.[3] Basically the system consists of a bakeable stainless steel ultrahigh-vacuum chamber equipped with an Extranuclear Laboratories, Inc., quadrupole mass spectrometer with a "Bessel box" energy prefilter, a Varian 0–3-keV ion bombardment gun, a Leybold-Heraeus, Inc., vertical turbomolecular pump, and a titanium sublimation pump. The base pressure is in the low 10^{-10} Torr range.

The samples used in this study consisted of distilled, deionized water and spectrograde benzene and cyclohexane which were degassed by repeated freeze–thaw cycles to a pressure of 1×10^{-9} Torr. The degassed samples were introduced into the chamber by means of a UHV valve that had a stainless steel tube welded to its inner side for conducting vapors to within 1 in. of the substrate on which the sample is to be deposited. The substrate was a 1-cm^2 99.95% platinum plate which was cooled to 77 K. Cooling is achieved by forcing liquid nitrogen through 0.0625-in. o.d., 0.001-in. walled stainless steel tubing into a reservoir in the carousel sample holder as illustrated in Figure 1. The tubing was coiled around the manipulator shaft in order to allow rotation of the carousel by ±180° and freedom of movement in three dimensions. A deposition period of 20 min during which the chamber pressure rose to 1×10^{-6} Torr resulted in the formation of a thick sample layer on the Pt plate. After deposition the chamber pressure fell again to 1×10^{-9} Torr.

Primary ion bombardment, with the ion gun situated 60° from the SIMS axis, was performed by backfilling the chamber with He to pressures over the range 1×10^{-8} to 1×10^{-6} Torr and using an emission current over the range 20–35 mA. Under these conditions ion currents over the ranges 5×10^{-9} to 3×10^{-7} A/cm^2 could be measured by means of a picoammeter. The low current ranges were obtained by reducing the emission current of the ion gun. This allowed maintenance of the rare gas pressure at $>1 \times 10^{-8}$ Torr, hence keeping the residual gas molecules to less than 1% of the total gas. Bombardment was performed under dynamic gas flow conditions with the turbomolecular pump open, thus providing a continuous stream of fresh He gas and removing sputtered products. The experiments

†Robert A. Welch Foundation Predoctoral Fellow.

0002-7863/79/1501-1951$01.00/0

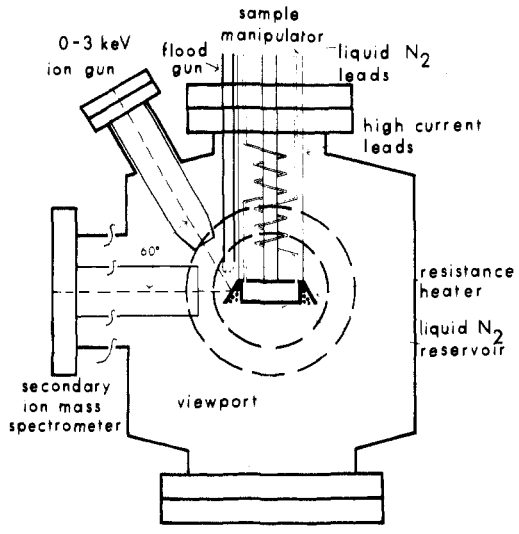

Figure 1. Schematic diagram of the spectrometer chamber showing the SIMS, sample carousel, liquid nitrogen cooling system, and ion bombardment gun.

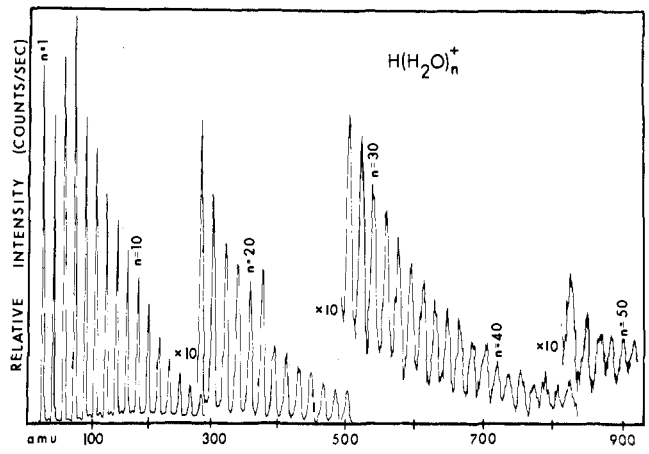

Figure 2. Positive SIMS of H_2O at 77 K obtained by bombardment with 3-keV, 1×10^{-8} A/cm^2 He^+ primary ions.

reported here were performed with primary ion currents $<1 \times 10^{-8}$ A/cm^2. Ne and Ar gases were also used for the primary ions; however, they tended to condense on the cold surface and yield intense interfering peaks such as Ne^+, Ne_2^+, etc.

Charging of these sample surfaces as a result of ion bombardment was substantial; compensation was provided by low-energy electrons from an electron flood gun. The flood gun filament was biased to −6 V below ground and the sample was maintained at ground potential. Electron emission currents over the range 10^{-10}–10^{-5} A were obtained by varying the current through the filament. The appropriate current was selected by maximizing the secondary ion signals as a function of flood gun current.

The energy prefilter used for kinetic energy measurements is an electrostatic "Bessel box" whose axis of symmetry is coincident with that of the quadrupole mass filter and is mounted directly in front of the latter. It enhances signal/noise and resolution by electrostatically drawing ions emitted from a source into its entrance aperture and by selecting a narrow band of kinetic energies for transmission. An intermediate stop precludes straight-line paths through the device. The potential of the main cylinder of the Bessel box retards the incoming ions and allows only those ions within a narrow energy range, i.e., the center pass band energy, to enter the quadrupole. All potentials, including the quadrupole rod reference, are fixed relative to the retarding potential so that the pass band can be varied without affecting the optics related to focusing and mass analyzing the ions. The transmission half-height band width is ~1.0 eV under optimum settings.

III. Experimental Results

A. H_2O. The positive SIMS of H_2O at 77 K is shown in Figure 2. A series of cluster ions of the type $H(H_2O)_n^+$, n = 1, 2, . . . , 51, can be observed. The quadrupole mass filter was tuned for optimum resolution at ~80 amu and was not adjusted during this spectral sweep; the degradation of resolution at higher masses is evident. Retuning the quadrupole at regular mass intervals can correct this situation at the expense of intensity modifications. The cluster intensities generally decrease monotonically throughout the long series. Plotting the logarithm of the cluster intensities vs. mass (Figure 3) yields a reasonably straight line which can be fit to an equation of the type

$$I = ae^{bn} \quad (1)$$

where I is the observed cluster intensity (counts/s), n is the number of H_2O molecules in the cluster, and a and b are parameters. Notable deviations from the monotonic decrease are particularly evident in Figure 2 for the clusters n = 3, 4, and 21. These anomalies must be attributable to the relatively

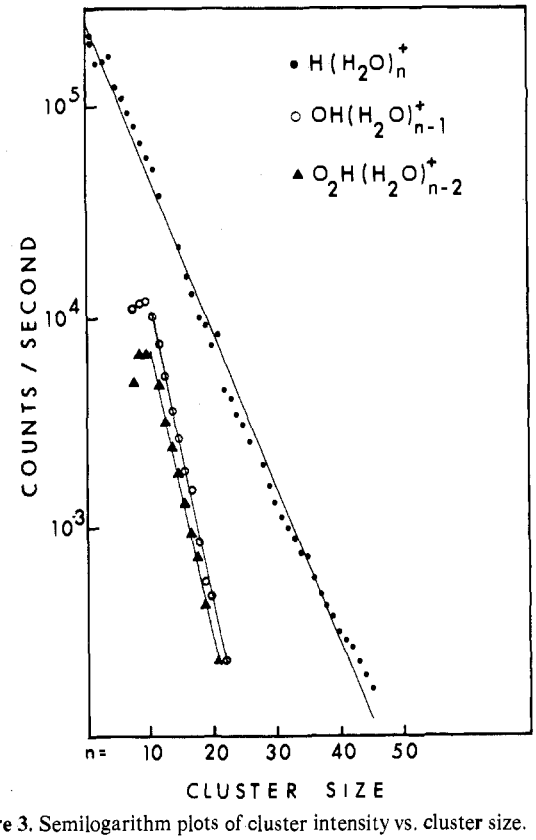

Figure 3. Semilogarithm plots of cluster intensity vs. cluster size.

higher stability of these particular clusters over their neighbors.

The kinetic energy distributions of some positive secondary ion clusters, $H(H_2O)_n^+$, are plotted in Figure 4. The distributions for the $n > 1$ clusters all have maxima near 2 eV and widths at half-height of ~1.5 eV. The n = 1 cluster has a distinctly higher maximum, i.e., 3.3 eV, and broader width, i.e., 2.5 eV. Our previous work on alkali halide[2,3] clusters showed that, in general, the maximum of the distribution is shifted to lower energy and is sharpened with increasing cluster size.

The variations of some representative $H(H_2O)_n^+$ cluster intensities as a function of primary ion energy are shown in Figure 5. These curves were obtained by using a band-pass energy of 10 eV, i.e., the complete distribution from 0 to 10 eV of Figure 4 was accepted. As primary ion energy decreases, the cluster intensity decreases more rapidly as cluster size in-

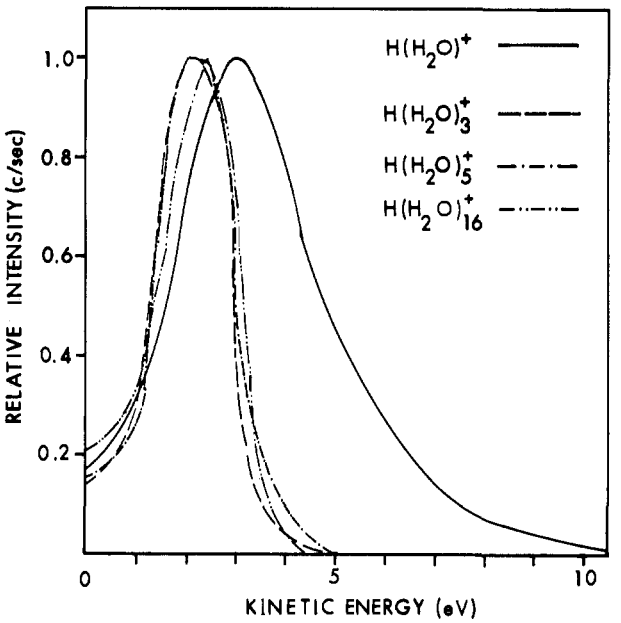

Figure 4. Kinetic energy distributions of the $H(H_2O)_n^+$ clusters.

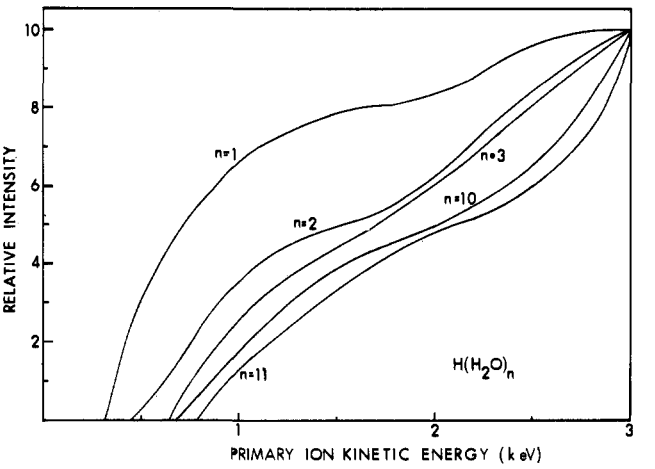

Figure 5. Relative intensities of some representative $H(H_2O)_n^+$ clusters as a function of primary ion kinetic energy. The intensities are all normalized to 10 at 3-keV kinetic energy.

creases. The lower limit of our detectability of the clusters (~300 eV for $H(H_2O)^+$) increases as cluster size increases (~780 eV for $H(H_2O)_{11}^+$).

Other types of H_2O clusters are observed, although with much weaker intensities than the above-mentioned ones. Figure 6 is a representative segment of the spectrum with increased sensitivity showing some of the different types of clusters. Clusters of the type $(HO_m)(H_2O)_{n-m}^+$, $m = 1, 2$, can be observed from $n = 8$ upward on the low-mass side of the $H(H_2O)_n^+$ peaks. Their intensities increase with increasing n to the limit of the quadrupole. A very weak series of the type $(H_2O)_n^+$, $n = 1, 2, \ldots, 5$, can be detected. Isotope peaks on the high-mass side of the major $H(H_2O)_n^+$ peaks are particularly evident for $n = 4$, 5, and 6 in Figure 6. Other low-intensity peaks situated midway between the $H(H_2O)_n^+$ peaks appear to be doubly charged clusters of the type $H_m(H_2O)_{2n+1}^{2+}$, $n = 1, 2, \ldots, 30$ and $m = 0, 1, \ldots, 7$. This observation indicates that the cluster size is not limited to $H(H_2O)_{51}^+$; this is only the approximate limit of the quadrupole analyzer. Peaks of H^+ and H_2^+ are also observed. The intensities of some of the $(HO_m)(H_2O)_{n-m}^+$ clusters are plotted in Figure 3; they go through a maximum and then decay exponentially. The slopes of the straight lines of Figure 3 are noticeably different for the different types of clusters. The negative SIMS of H_2O at 77 K exhibited only ions of the type H^-, H_2^-, O^-, OH^-, H_2O^-, O_2^-, HO_2^-, $H(HO_2)^-$, and $H_2(HO_2)^-$. Large clusters were not observed in the negative ion spectrum.

B. Benzene and Cyclohexane. The SIMS of benzene and cyclohexane at 77 K are shown in Figures 7–10. Groups of peaks are observed corresponding to $1, 2, \ldots, 32$ carbon atoms for benzene. The general low intensity of these spectra made it necessary to increase the transmission through the quadrupole and hence a lowering of resolution as exhibited in Figure 8. The overall intensity of the cyclohexane spectrum was approximately one order of magnitude lower than that of benzene. As a result of this low intensity of cyclohexane, the largest positive cluster observed was at ~212 amu and the largest negative cluster observed was C_3H^-. Positive and negative H and H_2 ions were observed from both benzene and cyclohexane, although they are not shown in the figures. The low-mass region of the benzene spectrum is very similar to the previously published[1] low-mass SIMS of benzene.

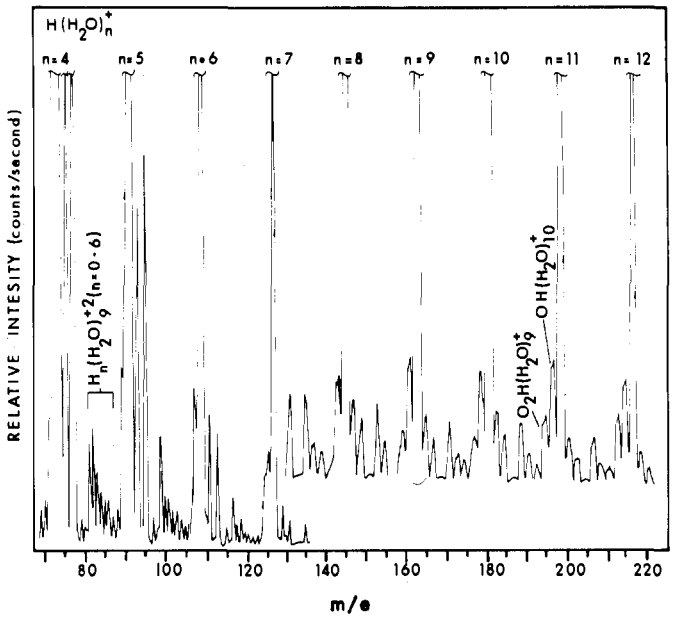

Figure 6. Segment of the positive SIMS of H_2O at 77 K with high sensitivity.

The number of hydrogen atoms in the clusters increases at low mass until eight to ten hydrogens per cluster is attained. Above this point, addition of carbons to the clusters occurs with no corresponding increase in the number of hydrogens. Such deviations in composition from that of the pure hydrocarbons are indicative of molecular rearrangement during sputtering. After extensive He^+ bombardment, a black residue was observed on both the benzene and cyclohexane surfaces. Analysis of this residue indicated a composition of pure carbon which was almost devoid of hydrogen.

The intensity distributions of the peaks in the gas-phase electron-impact mass spectra of benzene and cyclohexane, as measured with the same Extranuclear quadrupole, are distinctly different from the SIMS. The SIMS exhibit a much weaker molecular parent ion than the electron-impact spectra. The most abundant fragment in SIMS is the $C_3H_3^+$ ion for benzene and the $C_2H_3^+$ ion for cyclohexane, while in electron-impact spectra it is the molecular parent ion for benzene and the $C_4H_8^+$ ion for cyclohexane. The SIMS show peaks for

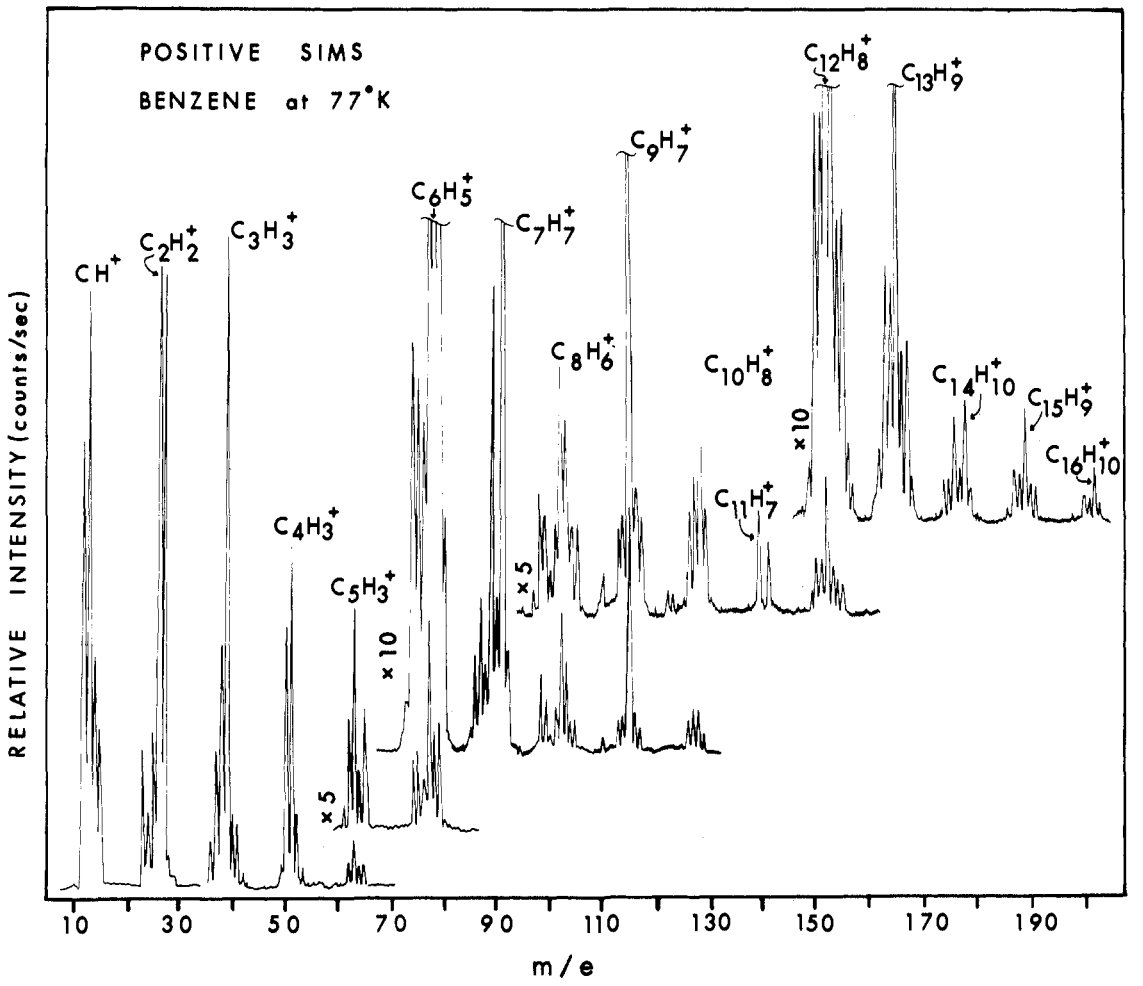

Figure 7. Low mass positive SIMS of benzene. The highest intensity peak is identified in each group.

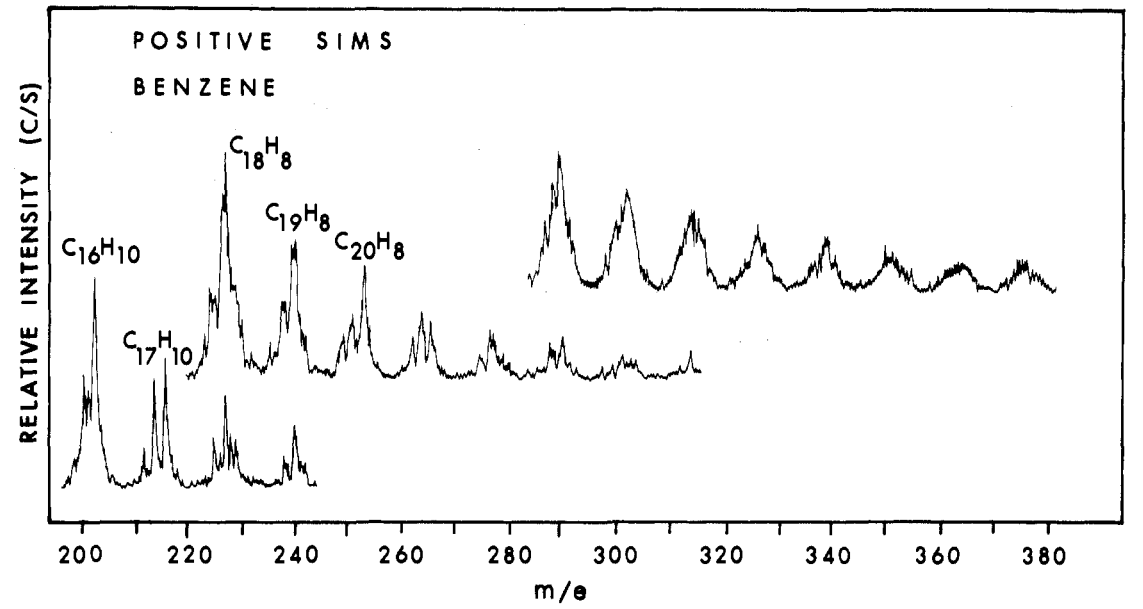

Figure 8. High mass positive SIMS of benzene. The highest intensity peak is identified in each group.

the $(M + 1)^+$ ions whose intensities are far greater than those of the natural ^{13}C isotope. The secondary ion energy distributions and their dependence on primary ion energy are similar to those of H_2O and are not reiterated here.

C. General Results. There is no doubt that the observed spectra originate from molecules on the surface of the cold probe and not from gas-phase species. This is particularly evident when one considers the low vapor pressures ($<10^{-9}$ Torr)

of the samples at 77 K. Experiments in which the frozen sample was rotated 180° and the ion beam struck the clean sample holder showed only ions of the stainless steel sample holder. The sample temperatures were varied from 77 to ~150 K with no detectable change in the relative fragment ion abundances. The spectra show excellent reproducibility and independence to the type of rare gas primary ion and its kinetic energy above ~800 eV. Increasing the primary kinetic energy seems only to increase the overall cluster intensity above this level.

IV. Discussion

The following general mechanism is proposed for a qualitative interpretation of the experimental results presented in the previous section. A single energetic primary ion collides with the surface and transfers its momentum in collision cascades to lattice atoms in the vicinity of the collision site. This results in a transient hemispherical region surrounding the impact site in which the energy content per unit volume is sufficient to thermally activate the constituent atoms. The random motion acquired by the lattice atoms in this region can propagate them out of the surface into the vacuum if their velocity vectors are in the appropriate direction and sufficiently large to overcome the surface binding energy. As such species propagate through the surface region *large molecular clusters can be formed if the species are so synchronized in space, time, and velocity such that the attractive potential energy between them is sufficiently large to bind them together as a single cluster entity.* Such clusters can undergo decomposition or rearrangement during their flight through the mass spectrometer. In order to discuss this process, it is instructive to partition the mechanism into the following steps: (A) primary ion impact, (B) momentum cascades and cluster formation, and (C) flight time. These steps in the mechanism will be discussed in more detail.

A. Primary Ion Impact. The secondary ions are produced by single primary ion collisions with the surface; multiple collisions by primary ions are insignificant. This can be exemplified by a simple computation. Using a primary ion current of 1×10^{-8} A/cm^2 there are about 6×10^{-6} ions/s·Å^2 impingent on the surface. If each ion distributes its energy over a site of 10-Å radius, then approximately 2×10^{-3} ions/s·site or one primary ion strikes the site every ~8 min. When the primary ion current is 1×10^{-6} A/cm^2, the time interval between collisions with a site is ~5 s. These time intervals are many orders of magnitude longer than the time required to dissipate the momentum of the primary ion and for the secondary ions to travel to the detector. This is supported by the observed[2-4] monotonic decrease in secondary ion intensity as primary ion current decreases, indicating that the sputtering mechanism and cluster formation process do not change to a detectable extent over the range studied.

B. Momentum Cascades and Cluster Formation. The collision of the energetic primary ion with the surface is similar to that of billiard balls in which atoms of the lattice absorb the primary momentum in a cascade process. The momentum is transferred to lattice atoms as the cascade propagates in random directions. The time interval of such a dissipation process is of the order of several vibrational periods, i.e., 10^{-13} s. The nonequilibrium situation induced by a large amount of energy deposited almost instantaneously in a localized hemispherical region can be relieved by an irreversible adiabatic expansion into the vacuum. Species in the localized region that acquire velocity vectors near the surface normal can leave the lattice and enter into the vacuum if their energies are greater than the surface binding; those that acquire velocity vectors which form small angles with the surface can be recaptured by the surface, resulting in ion beam induced migration of surface species.

The question that arises from this is *whether the large clusters are ejected as single entities resulting from contiguous sites on the surface or they are ejected as species from both adjacent and nonadjacent atomic sites which are a result of atomic recombination in the thermally activated region.* We believe the latter to be the best description of the process and propose the following mechanism for large cluster formation.

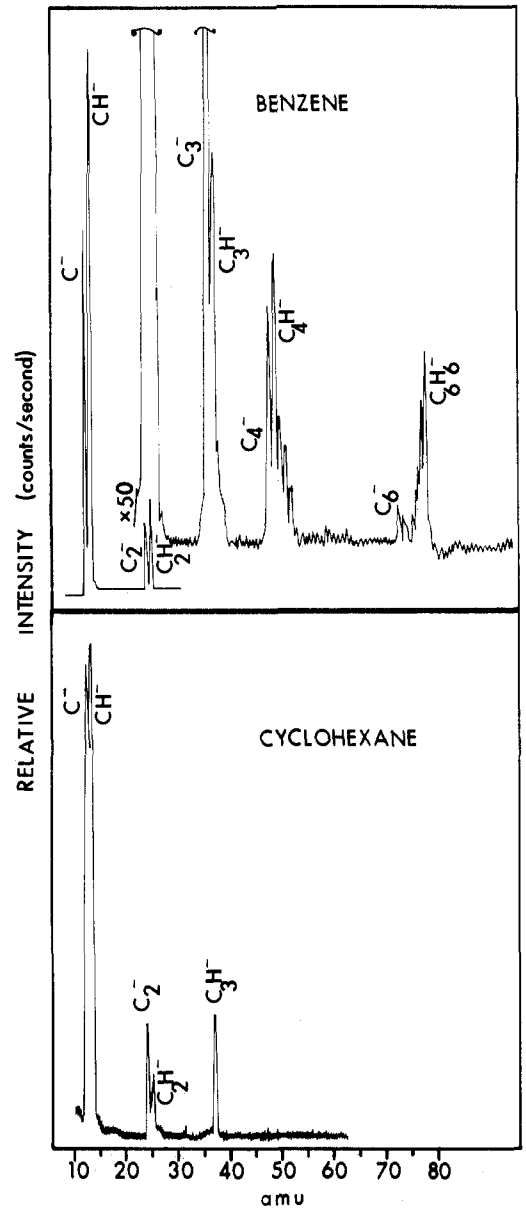

Figure 9. Negative SIMS of benzene and cyclohexane. The highest intensity peak is identified in each group.

The species moving randomly in the activated region will consist of atomic and molecular ions of both polarities as well as neutrals with a broad velocity distribution determined by the momentum transferred. The local density of such species in this region will be very high, i.e., similar to the atomic density of the original crystal. The high density of such species will result in significant attractive and repulsive potentials in this small spatial region. If we consider a collection of particles moving in the activated region that are closely synchronized in space and time, they can be bound together as a cluster if they satisfy the relationship

$$\sum_{i,j} (E^k{}_{i,j} + V_{i,j}) < 0 \qquad (2)$$

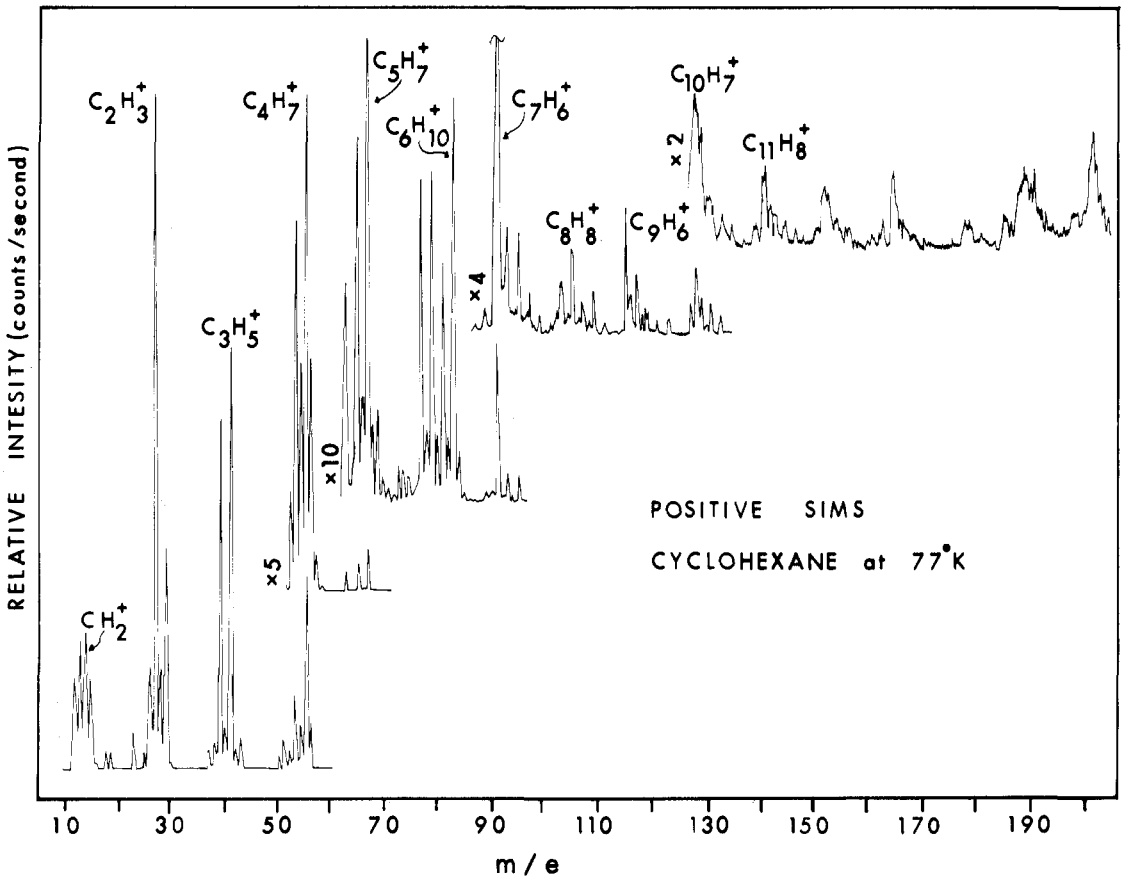

Figure 10. Low mass positive SIMS of cyclohexane. The highest intensity peak is identified in each group.

where $E^k_{i,j}$ is the relative kinetic energy of the particles i,j and $V_{i,j}$ is the potential energy between each pair of particles i,j. From eq 2, particles that have large electrostatic attraction or chemical affinity between them will result in large negative $V_{i,j}$'s which will dominate over the $E^k_{i,j}$ terms and yield a bound cluster. As a result, a single primary ion collision can generate a collection of particles moving through the surface which can be bound together in one or more different clusters according to eq 2. This process has recently been modeled[18] by computer simulation of the classical trajectories in sputtering.

Consider, for example, the formation of $H(H_2O)_{51}^+$ from a 1-keV He^+ collision. Using the lattice spacing of ice, a $H(H_2O)_{51}^+$ cluster would have a volume of approximately 1.6 × 10^5 Å^3. If such a cluster would be ejected from a hemispherical region just below the surface, the radius of the hemisphere would be ~42 Å. Using heat-capacity data for H_2O and assuming that all of the primary energy is deposited in this hemisphere, it is easily shown that effective temperatures of many billions of degrees can be obtained. It is not likely that all of the primary energy is deposited in this small volume, for a single primary ion collision could result in the production of several different clusters. Even at effective temperatures of ~10^6 °C, the average velocities of oxygen and hydrogen atoms are in the range of 10^6–10^7 cm/s. The atomic density of ice corresponds to an effective pressure of ~10^7 atm at which the mean free path of the activated atoms is only ~3 Å. Under such conditions there are ~5 × 10^{14} collisions/s and a cluster such as $H(H_2O)_{51}^+$ could be formed in ~10^{-13} s even if 150 single atom interactions are required.

The formation of a tightly bound cluster only after the particles are moving through the selvedge region of the surface is supported by the following observations. Firstly, the fit of eq 1 (Figure 3) for each individual type of cluster suggests that the slope b is related to the relative rate of formation of each cluster type and the intercept a represents the relative stability or lifetime of such clusters after formation. Secondly, consider two particles with momentum vectors $\mathbf{m}_1\mathbf{v}_1$ and $\mathbf{m}_2\mathbf{v}_2$ that interact to form a single moiety with momentum vector $(\mathbf{m}_1 + \mathbf{m}_2)\mathbf{V}$, where $\mathbf{V}$ denotes the velocity of the cluster. Considering the magnitudes of these vectors, with conservation of momentum, we find that

$$\mathbf{m}_1(\mathbf{v}_1 - \mathbf{V}) + \mathbf{m}_2(\mathbf{v}_2 - \mathbf{V}) > 0 \qquad (3)$$

such that $\mathbf{V}$ must always be less than the larger of the particle velocities $\mathbf{v}_1$ or $\mathbf{v}_2$. The general sharpening and shift to lower energy of the kinetic energy distributions (Figure 4) as cluster size increases observed in the alkali halides[2,3] and the significantly different behavior of $H(H_2O)^+$ from the $H(H_2O)_n^+$ clusters may be a result of several such required interactions to form large clusters. The broad high-energy distribution of $H(H_2O)^+$ suggests that it is ejected directly from the surface while the sharper low-energy distributions of the larger clusters suggest that they are produced by a recombination mechanism of the type

$$H_2O + H(H_2O)_{n-1}^+ + S \rightleftarrows H(H_2O)_n^+ + S \qquad (4a)$$

and

$$H(H_2O)_i^+ + (H_2O)_j + S \rightleftarrows H(H_2O)_n^+ + S,\ i + j = n \qquad (4b)$$

where S is the third body. This third body can be the surface itself and is required for the deactivation of the initially excited association products and for the activation of clusters in decomposition reactions. Similar reactions of benzene fragments

with parent molecules can be postulated. For example, the abundant ions $C_3H_3^+$, $C_5H_3^+$, and $C_5H_5^+$ can add to neutral benzene with elimination of H_2 to yield the observed ions $C_9H_7^+$, $C_{11}H_7^+$, and $C_{11}H_9^+$. On the other hand, odd-electron ions such as $C_4H_2^+$ can add without H_2 elimination to yield $C_{10}H_8^+$. However, exceptions to this can be found and such specific mechanistic details are at present purely speculative. We do not wish to imply equilibrium by eq 4; the clustering environment changes so rapidly in the sputtering region that the clusters cannot be in equilibrium with their surroundings. Thirdly, the rapid decrease in cluster intensity as the primary ion energy decreased below ~1 keV suggests that below this point the energy deposited per unit volume is small and hence larger cluster formation is improbable. Fourthly, it has been observed[3,5] that atoms which are two to four atomic sites apart in the lattice can be ejected in a single cluster without inclusion of the intermediate atoms in the cluster. Evidence[3,5] for this is contained in the alkali halide, MX, spectra where species such as M_n (n = 2, 3) are observed and in the spectra of $CsClO_4$, $NaBF_4$, and KPF_6, where species such as $M_nX_{n-1}^+$ (n = 1, 2, . . .) are observed. Such observations indicate that nonadjacent lattice atoms are combining to form clusters, i.e., there is significant molecular rearrangement as a result of the sputtering process.

C. Flight Time. The positive or negative cluster ions emanating from the surface can be electrostatically drawn into the SIMS spectrometer for a total flight path from sample to detector of ~42 cm. The ions travel through the prefilter and quadrupoles at low kinetic energies. Assuming an ion energy of ~2 eV and mass of ~900 amu (for the large water clusters), the flight time and minimum lifetime of the clusters is ~0.6 ms. During this period, unstable or highly vibrationally excited clusters can decompose into smaller fragments. The large deviations of some of the points in Figures 2 and 3 from the straight lines indicate that certain clusters do have abnormally high stabilities.

D. Relation to Previous Work and Applications. The unusually high intensities of the $H(H_2O)_4^+$ and $H(H_2O)_{21}^+$ clusters (Figure 2) and their deviations from the monotonic intensity decrease suggest that these clusters have unusual stability. These abnormal stabilities have been observed[19,20] previously in free jet adiabatic expansions of liquid water. The $H(H_2O)_4^+$ cluster is believed to be a symmetrical H_3O^+ ion surrounded trigonally by three H_2O molecules. The $H(H_2O)_{21}^+$ cluster is attributed[19] to a clathrate cage structure, i.e., a pentagonal dodecahedron with a water molecule at each corner and an H_3O^+ ion at the center. The fact that our $H(H_2O)_n^+$ intensity distributions (Figure 2) are very similar to those obtained from expansion of liquid water (see ref 19, Figure 1) lends strong support to the proposed mechanism in which a localized surface region is thermally activated and recombination occurs. The emission of clusters from this region is apparently not unlike the adiabatic expansion of liquid water.

Our results show that there is adequate sensitivity for characterization of molecular solids and, even though the fragmentation appears to be stronger than in electron-impact mass spectra, the fragmentation patterns do allow organic structure determination. Despite the recombination, SIMS does provide a qualitative fingerprint for the compounds. SIMS can, in principle, be performed in two modes:[7-10] the "static" and "dynamic" mode. In static SIMS the primary ion flux is low enough to avoid sputtering away the outer monolayer of the surface during the measurement period, while in dynamic SIMS the surface is eroded faster than the measurement period. The condition usually accepted for the static SIMS mode is a primary ion flux of less than 1×10^{-8} A/cm^2. We point out that the conditions for static SIMS will depend largely on the type of surface being studied. Obviously, surfaces that emit 154 atom clusters will be eroded faster than those that emit only atomic or small molecular species. The recent observation[26] of very large erosion coefficients (far larger than those expected from normal sputtering processes) for ice subjected to megaelectron volt ion bombardment will certainly have to be explained in this manner. Static SIMS conditions for one sample may very well be dynamic SIMS conditions for another sample.

The existence of large stable ionic clusters and their production by low-flux rare gas sputtering of molecular solids have important applications to astrophysical studies of clustering in the upper atmosphere, as reactants in charge or proton exchange reactions,[27] as a technique for volatilization and mass analysis of large involatile molecules,[28] and possibly as a method of injecting fuel into thermonuclear devices.[29] Large sputtering coefficients for molecular frosts may be important to the balance of planetary atmospheres, to determining the size distribution of interplanetary ice particles, and in the dynamics of comet structures.

V. Conclusions

We have shown that large molecular clusters of high mass can be sputtered from molecular solids and detected by the method of SIMS. The fragmentation is stronger than in the electron-impact mass spectrum; however, the patterns can be used to determine the molecular structure. The experimental results are consistent with a clustering mechanism in which a collection of particles is thermally activated by the collision of a single primary ion. The resulting nonequilibrium situation in which a large amount of energy is deposited almost instantaneously into a localized region can be relieved by an irreversible adiabatic expansion into the vacuum. The activated species can take the form of a bound cluster as they move through the selvedge region of the surface. The delayed formation of a tightly bound cluster until the particles are moving through the surface accounts for the observed molecular rearrangement, the preponderant specific cluster types, and the possibility of clusters containing atoms from noncontiguous lattice sites. However, since equilibrium is not established in the activated region, the secondary clusters will reflect to some degree the short-range lattice structure. As a result, the technique does provide a fingerprint for species such as hydrocarbons, complex salts, etc.

Acknowledgment is made to the U.S. Army Research Office and the Energy Laboratory of the University of Houston for support of this work.

References and Notes

(1) H. T. Jonkman, J. Michl, R. N. King, and J. D. Andrade, *Anal. Chem.*, **50**, 2078 (1978).
(2) G. M. Lancaster, F. Honda, Y. Fukuda, and J. W. Rabalais, *Int. J. Mass Spectrom. Ion Phys.*, in press.
(3) F. Honda, G. M. Lancaster, Y. Fukuda, and J. W. Rabalais, *J. Chem. Phys.*, **69**, 4931 (1978).
(4) F. Honda, G. M. Lancaster, and J. W. Rabalais, *Surf. Sci.*, **76**, L613 (1978).
(5) J. A. Taylor and J. W. Rabalais, *Surf. Sci.*, **74**, 229 (1978).
(6) R. W. Hewitt, A. T. Shepard, W. E. Baitinger, N. Winograd, G. L. Ott, and W. N. Delgass, *Anal. Chem.*, **50**, 1286 (1978).
(7) A. Benninghoven, O. Ganschow, and L. Wiedmann, *J. Vac. Sci. Technol.*, **15**, 506 (1978).
(8) S. Taya, H. Tsuyama, M. Itoh, and I. Kanomata, *Mass. Spectrom.*, **25**, 251 (1977).
(9) P. H. Dawson, *Surf. Sci.*, 71, 247 (1978); **65**, 41 (1977); **57**, 229 (1976); *Phys. Rev. B.*, **25**, 5522 (1977).
(10) A. Benninghoven and A. Müller, *Surf. Sci.*, **39**, 416 (1973); M. Barber, J. C. Vickerman, and J. Wolstenhole, *J. Catal.*, **42**, 48 (1976).
(11) M. L. Yu, *Surf. Sci.*, **71**, 121 (1978); *Nucl. Instrum. Methods*, **149**, 559 (1978).
(12) H. W. Werner, *Surf. Sci.*, **47**, 301 (1975).
(13) H. Liebl, *J. Vac. Sci. Technol.*, **12**, 385 (1975).
(14) P. Sigmund, *Phys. Rev.*, **84**, 383 (1969); J. N. Coles, *Surf. Sci.*, **55**, 721 (1976); M. J. Dresser, *J. Appl. Phys.*, **39**, 338 (1968); J. M. Schroeer, T. H. Rhodin, and R. C. Bradley, *Surf. Sci.*, **34**, 571 (1973); M. Cini, *ibid.*, **54**, 71 (1976); C. A. Anderson and J. R. Hinthorne, *Anal. Chem.*, **45**, 1421 (1973).

(15) G. P. Können, A. Tip, and A. E. deVries, *Radiat. Eff.*, **21**, 269 (1974); **26**, 23 (1975); Z. Jurela, *Int. J. Mass Spectrom. Ion Phys.*, **12**, 33 (1973); F. G. Rudenauer, W. Steiger, and H. W. Werner, *Surf. Sci.*, **54**, 553 (1976); M. Szymonski and A. E. deVries, *Phys. Lett. A*, **63**, 359 (1977); G. Blaise and G. Slodzian, *Rev. Phys. Appl.*, **8**, 105 (1973).
(16) D. E. Harrison, Jr., and C. B. Delaplain, *J. Appl. Phys.*, **47**, 2252 (1976).
(17) N. Winograd, D. E. Harrison, Jr., and B. J. Garrison, *Surf. Sci.*, **78**, 467 (1978).
(18) B. J. Garrison, N. Winograd, and D. E. Harrison, Jr., *J. Chem. Phys.*, **69**, 1440 (1978).
(19) S. S. Lin, *Rev. Sci. Instrum.*, **44**, 516 (1973); J. Q. Searcy and J. B. Fenn, *J. Chem. Phys.*, **61**, 5282 (1974); R. R. Burke and R. P. Wayne, *Int. J. Mass Spectrom. Ion Phys.*, **25**, 199 (1977); J. L. Kassmer, Jr., and D. E. Hagen, *J. Chem. Phys.*, **64**, 1860 (1976).
(20) P. Kebarle in "Ion Molecule Reactions", J. L. Franklin, Ed., Plenum Press, New York, 1972, Chapter 7.
(21) J. Estel, H. Hoinkes, H. Kaarmann, H. Nahr, and H. Wilsch, *Surf. Sci.*, **54**, 393 (1976).
(22) I. G. Higginbotham, T. E. Gallon, M. Prutton, and H. Tokutaka, *Surf. Sci.*, **21**, 241 (1975).
(23) W. H. Weinberg, *Adv. Colloid Interface Sci.*, **4**, 301 (1975).
(24) A. K. Green and E. Bauer, *J. Appl. Phys.*, **39**, 2769 (1968).
(25) This general sharpening and shift in the kinetic energy distributions to lower energy as the cluster size increases have also been observed in the SIMS spectra from alkali halide crystals.[3,4]
(26) W. L. Brown, L. J. Lanzerotti, J. M. Poate, and W. M. Augustyniak, *Phys. Rev. Lett.*, **40**, 1027 (1978).
(27) R. J. Beuhler, E. Flanigan, L. J. Green, and L. Friedman, *J. Am. Chem. Soc.*, **96**, 3990 (1974).
(28) H. U. Winkler and H. D. Beckey, *Biochem. Biophys. Res. Commun.*, **46**, 391 (1972).
(29) W. Henkes, *Z. Naturforsch. A*, **16**, 842 (1961).

Enthalpies of Interaction of Aliphatic Ketones with Polar and Nonpolar Solvents

P. P. S. Saluja, L. A. Peacock, and R. Fuchs*

Contribution from the Department of Chemistry, University of Houston, Houston, Texas 77004. *Received August 17, 1978*

Abstract: Solvation enthalpies [$\Delta H(v \rightarrow S)$] of a variety of aliphatic ketones including straight-chain, branched, and cyclic compounds have been determined in methanol, dimethylformamide, benzene, and cyclohexane by combining measurements of the heats of solution (ΔH_s) and heats of vaporization (ΔH_v). Values of ΔH_v have been determined by the gas chromatography–calorimetry method, and several of the calculated liquid heat capacities required by this procedure have been verified by experimental measurement. $\Delta H(v \rightarrow S)$ for most ketones are in the order benzene (most exothermic) > DMF > MeOH > c-C_6H_{12}. Comparison of $\Delta H(v \rightarrow S)$ values for ketones with values for hydrocarbons of the same carbon skeleton provides a measure of polar interactions of the ketones with solvents. These interactions are largest for the cyclic and 2-ketones, less for the straight-chain symmetrical ketones, and least for the highly branched 2,2,4,4-tetramethyl-3-pentanone, and decrease with increasing ketone size within each group.

Gas-phase studies of solutes, complemented by measurements of the interactions of gaseous species with solvents, have been revived in recent years as a very important approach to an understanding of the intermolecular forces in solutions.[1-3] The significance of these studies to the understanding of solution reactivity and equilibria has been a subject of recent discussions by Taft[4] and Arnett.[5] A considerable research effort has been made in this laboratory to determine the extent to which aromatic compounds[6,7] with a variety of substituent groups, relatively nonpolar aliphatic hydrocarbons,[8] and functional groups introduced into the latter molecules[8,9] interact with polar and nonpolar solvents, in order to evaluate the major intermolecular forces operative in these solutions. The choice of solvents has been limited to nonaqueous ones, thus avoiding several additional complications encountered in aqueous solutions.[2]

The first step toward this goal must be to form a minimum number of empirical generalizations to describe intermolecular interactions, based on an extensive set of data, describing the effects of systematic changes in the structural features of the solute in a variety of polar and nonpolar solvents. The initial investigation in this direction has been carried out by the measurement of enthalpies of solution (ΔH_s) of series of alkanes and alkenes, including straight-chain, branched, and cyclic compounds, in polar solvents (methanol and dimethylformamide), nonpolar but highly polarizable benzene, and nonpolar cyclohexane.[8] There is strong experimental support for one empirical generalization, the existence of methylene group additivity[10] in the solvation enthalpies, $\Delta H(v \rightarrow S)$, and also in ΔH_s values of alkanes and alkenes. This study showed that alkenes are more strongly solvated than the corresponding alkanes in polar DMF, presumably because of dipole-induced dipole interactions of the solvent with the polarizable π bond of the alkenes, but the alkene–alkane difference in nonpolar cyclohexane is negligible, indicating that in cyclohexane both alkenes and alkanes are solvated almost entirely by dispersion forces. In polar solvents alkenes interact by dispersion, dipole-induced dipole, and perhaps very slightly by dipole–dipole forces, whereas alkanes interact with polar or nonpolar solvents almost entirely by dispersion forces. (In highly polar solvents dipole-induced dipole forces may make a small contribution.) The results were consistent with the premise that a given hydrocarbon group will make the same contribution to dispersion interactions regardless of the nature of the molecule of which it is a part. There is also strong evidence supporting a second empirical generalization,[8] that straight-chain hydrocarbons are better solvated in polar or nonpolar solvents than are branched isomers, and $\Delta H(v \rightarrow S)$ of alkanes are reduced by nearly 1 kcal/mol for each quaternary carbon atom present in the chain, arising from steric hindrance to solvation by dispersion forces. An additional reduction in the solvation of *trans*-1,2-di-*tert*-butylethylene was also observed, where steric factors prevent the close approach of the solvent dipoles to the π bond of the alkene, thereby diminishing the alkene–alkane difference in $\Delta H(v \rightarrow$ polar solvents).

These results are qualitatively consistent with a division of the observed overall enthalpies of solute–solvent interaction [$\Delta H(v \rightarrow S)$] into three terms: the enthalpy of cavity formation (ΔH_c) within the solvent (required to accommodate solute molecules); $\Delta H_{nonpolar}$, arising from dispersion forces; and the enthalpy of polar interactions (ΔH_{polar}) which arise from additional electrostatic interactions (dipole-induced dipole, di-

0002-7863/79/1501-1958$01.00/0